# SPH 法を用いたコンクリート版の貫通限界に関する基礎的検討

A fundamental approach on the penetration limit of concrete slab using SPH method

路馳*, 園田佳巨**
Chi Lu*, Yoshimi Sonoda**

*工修, 九州大学学生, 工学府建設システム工学専攻（〒819-0395 福岡市西区元岡 744 W2-1102）
**工博, 九州大学教授, 工学府建設システム工学専攻（〒819-0395 福岡市西区元岡 744 W2-1102）

*Keywords: RC slab, SPH analysis, penetration limit, high-velocity impact*
*キーワード : RC スラブ, SPH 解析, 貫通限界, 高速衝突*

## 1. INTRODUCTION

In recent years, to prevent serious damage from natural disasters such as tornados and volcanic eruptions, the demand for protecting structures against the collision of flying objects is widely recognized in Japan. U.S. Nuclear Regulatory Commission has already established design code considering the collision of flying objects towards nuclear facilities[1]. As for the volcanic eruption, because of the accident at Mt. Ontake volcano on September 27, 2014, in Japan, the design method of protective structures was re-examined and accurate evaluation for the impact resistance performance of protective structures against flying objects is required. For the existing studies on the local failure prevention measure, Beppu et al. [2] performed collision with a mushroom-shaped projectile on concrete plates. Kojima[3] conducted a set of tests with various RC slab targets and projectiles, inferring that the local damage of RC slab is the most related to the hardness of projectile's nose and more reinforcement would reduce local damage against hard-nose projectile. M.H Zhang et al. [4] pointed out that the penetration depth and crater diameter of high-strength concrete due to collision can be reduced by the increase of compressive strength and the presence of coarse granite aggregates.

Formulae have been developed based on experimental results, to predict the penetration depth and the critical slab thickness for perforation and scabbing of reinforced concrete to occur. Kennedy[5] compared and reviewed formulae of modified Petry, ACE (Army Corps of Engineers), BRL (Ballistic Research Laboratory), modified NDRC (National Defense Research Committee) and Ammann and Whitney and the Ballistic Research Laboratory.

For existing studies, the penetration limit of a concrete slab has been examined by experiments, while impact tests were usually performed by small scale specimens due to the limitation of experimental conditions. Furthermore, it is still difficult to predict the accurate local failure of the concrete structure. The use of numerical analysis is a powerful alternative to study impact phenomena in term of scale and cost. In general, FEM is not suitable to simulate the discontinuous displacement field such as penetration process. Therefore, Smoothed Particle Hydrodynamics (SPH) as one of the particle methods that can reproduce local failure of concrete structural members such as crushing or penetration is utilized. SPH is a particle-based Lagrangian method for solving systems of partial differential equations. Since its invention, it has been successfully applied to a vast range of problems such as the dynamic response of material strength[6,7], fluid flow8], etc.

In this study, SPH method is used to express the local failure of concrete, and the effect of influence domain and erosion limit to penetration process is discussed through the analysis results.

## 2. METHODOLOGY

### 2.1 SPH analysis

In this study, SPH method, which is one of the most popular mesh-free methods, is adopted in order to analyze local failure phenomena of concrete which are difficult to simulate by FEM. As shown in Fig.1(a), when large deformation problems are solved by FEM, there is a high possibility of finite elements distortion resulting in a non-negligible numerical error in the interpolation of displacement field using shape function. On the other hand, SPH is a method of discretizing a solid body as a large collection of particles and it is easy to express large distorted condition as shown in Fig.1(b). The physical quantity of each particle is evaluated by the weighted mean of the adjacent particles using the kernel function as shown in Fig.1(c) and basic equation of the SPH method is written as Eq.(1).

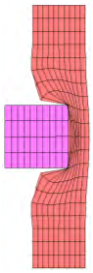

**Fig. 1(a)** FEM with large mesh deformation

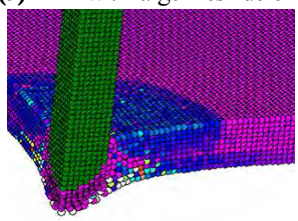

**Fig. 1(b)** SPH with particle discretization

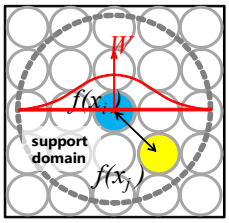


**Fig. 1(c)** SPH approximations calculation

$$\langle f(x_i)\rangle = \int_{\Omega} f(x_i)W(x_i - x_j, h)dx_j \qquad (1)$$

where $W$ is the kernel function, $h$ is the smoothing length, terms inside angel bracket are SPH approximations, $\Omega$ is the integral area within the support domain and $x_{i,j}$ are the position of particle $i$ and $j$. For the collision between objects, the impact force is calculated by the ratio of overlap area of particles using the pin-ball algorithm concept. Central difference method is used as the time integration method for the dynamic process, and the time step is $10^{-7}$s.

### 2.2 Material model

To analyze the elastic-plastic behavior of concrete, pressure-dependent yield function such as Drucker-Prager's equation is often used for the yield criteria. However, it is well known that linear Drucker-Prager's yield surface overestimates compressive strength of concrete under high hydrostatic pressure condition. Therefore, non-linear Drucker-Prager's yield function[2] which improves linear Drucker-Prager's equation is applied in this study. Non-linear Drucker-Prager yield function is represented by the following Eq. (2).

$$f(I_1, J_2) = \sqrt{J_2} - \sqrt{\frac{\gamma^2 - \alpha\beta I_1}{3}} = 0 \qquad (2)$$

where, $I_1$ is the primary invariant of stress, $J_2$ is the second invariant of deviatoric stress, $\alpha$ is a constant determining the yielding surface, $f_c$ is the uniaxial compressive strength, $f_t$ is the uniaxial tensile strength, $\gamma$ is $\sqrt{f_c f_t}$ and $\beta$ is $(f_c - f_t)$.

Fig. 2(a) shows non-linear Drucker-Prager yield surface in the $\sqrt{J_2} - I_1$ plane. In this study, to achieve a narrower yielding surface, $\alpha = 1$ in compression, and $\alpha = \sqrt{3}$ in tension are adopted, respectively.

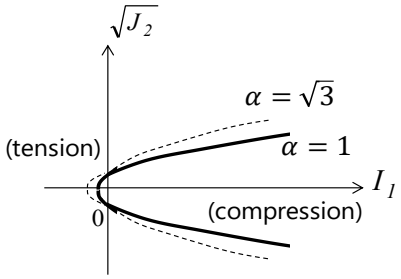


**Fig. 2(a)** nonlinear Drucker-Prager yield criterion

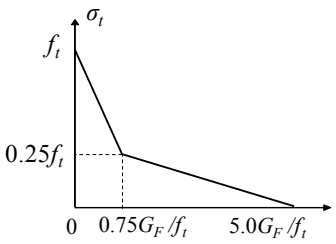


**Fig. 2(b)** Tensile bilinear softening

Furthermore, bilinear softening is considered on the tensile stress side according to the Japanese specification[9], as shown in Fig. 2(b), where $\sigma_t$ is the tensile stress, w is crack width, $f_t$ is the tensile strength of concrete, and $G_F$ is the fracture energy of concrete.

Compressive softening is also considered according to Popovic's equation[10], as shown in Eq.(3).

$$\sigma_{pr} = f_c \cdot \frac{n\left(\frac{\varepsilon_{pr}}{\varepsilon_{co}}\right)}{(n-1) + \left(\frac{\varepsilon_{pr}}{\varepsilon_{co}}\right)^n}$$
$$\varepsilon_{co} = \frac{f_c}{E_c\left(1 - \frac{1}{n}\right)}, n = \exp(0.0256 \cdot f_c) \qquad (3)$$

Where $f_c$ is the uniaxial compressive strength, $\varepsilon_{pr}$ is the principal strain, and $\varepsilon_{co}$, $n$ are parameters determined from material tests. Hardening is considered on the compression stress side as shown in Eq. (4).

$$H = \frac{d\sigma}{d\varepsilon^p} \qquad (4)$$

Where $d\sigma$ is equivalent stress increment, $d\varepsilon^p$ is equivalent plastic strain increment.

In addition, anisotropic damage in tensile and compression side is also introduced by sigmoid function (Eq. (5)) and Popovic's equation (Eq. (6)), respectively.

$$D_{pr} = \frac{D_{\lim}}{1 + \exp\left[-k\left(\varepsilon_{pr}^{p} - \frac{\varepsilon_{max}^{p}}{2}\right)\right]}, \quad (0 \le D_{pr} \le 0.4) \tag{5}$$

$$D_{pr} = \frac{n\left(\frac{\varepsilon_{pr}}{\varepsilon_{co}}\right)}{(n-1) + \left(\frac{\varepsilon_{pr}}{\varepsilon_{co}}\right)^{n}}, \quad (0 \le D_{pr} \le 0.2) \tag{6}$$

Where $D_{pr}$ is the damage along the principal direction; $k$ is the gradient adjustment constant, and $k = 300$ in this study; $\varepsilon_{pr}^{p}$ is the equivalent plastic strain along the principal direction; $\varepsilon_{max}^{p}$ is the maximum limit of equivalent plastic strain, and $\varepsilon_{max}^{p} = 0.03$. The damage-principal strain relationship is shown in Fig.3.

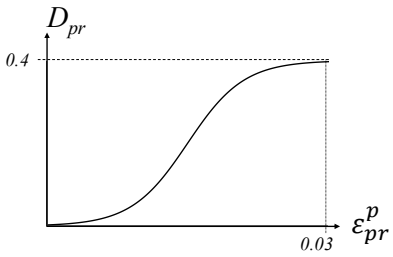


**(a)** Tensile

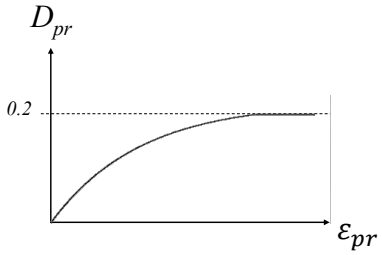


**(b)** Compressive

**Fig. 3** The damage-principal strain relationship

To obtain the elastic stiffness matrix with damage, the damage in the global coordinate is calculated first with $D_{pr}$ using the following equation:

$$D_i = \sum_{i=1}^{3} \left| D_{pr} e_{i,pr} \right|, (i = 1, 2, 3) \tag{7}$$

Where $D_i$ is the damage in global coordinate, $e_{i,pr}$ is unit vector of principal direction. The above calculation process is shown in Fig.4

Then the decrease ratio of elastic stiffness $d_{ij}$ is calculated by the following equations:

$$d_{ij} = \sqrt{(1 - D_i)(1 - D_j)} \tag{8}$$

Finally, the elastic stiffness matrix can be written as Eq. (9), where $\lambda = \nu E/[(1+\mu)(1-2\mu)]$, $\mu = E/[2(1+\nu)]$, and $E$, $\nu$ are the Young's modulus and the Poisson's ratio, respectively.

In this study, when the volumetric strain of concrete particle $\varepsilon_v$ reaches erosion limit $\varepsilon_{v\_lim}$, the particles are regarded as a crushing condition and the stress and stiffness of the particle are assumed to be zero, however, the particle itself is not erased to keep the mass conservation. The uniaxial stress-strain relationship of concrete is schematically shown in Fig. 5.

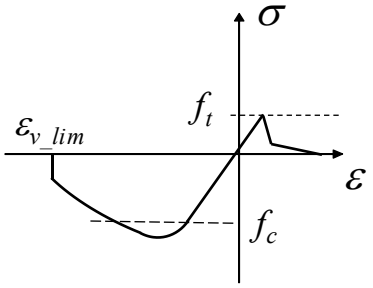


**Fig. 5** Uniaxial stress-strain relationship of concrete

Since the main subject of this study is to simulate the penetration process, strain rate effect of concrete is introduced by dynamic increase factors calculated by Fujikake's equation11) (in tensile stress) and Rose's equation[12] (in compression stress), shown in Eq. (10) and Eq. (11), respectively.

$$E^{e} = \begin{pmatrix} (\lambda+2\mu)d_{11} & \lambda d_{12} & \lambda d_{13} & 0 & 0 & 0 \\ \lambda d_{12} & (\lambda+2\mu)d_{22} & \lambda d_{23} & 0 & 0 & 0 \\ \lambda d_{13} & \lambda d_{23} & (\lambda+2\mu)d_{33} & 0 & 0 & 0 \\ 0 & 0 & 0 & 2\mu d_{12} & 0 & 0 \\ 0 & 0 & 0 & 0 & 2\mu d_{23} & 0 \\ 0 & 0 & 0 & 0 & 0 & 2\mu d_{13} \end{pmatrix} \tag{9}$$

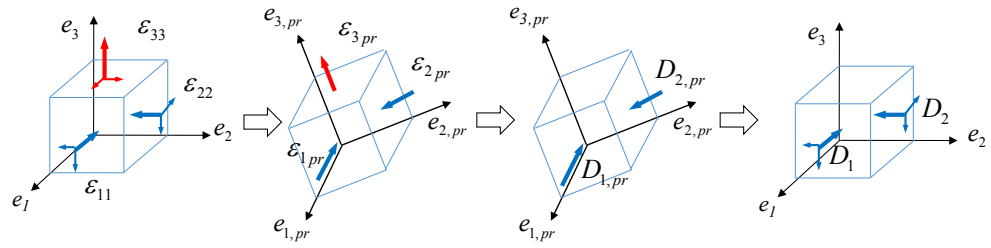


Strain components in global coordinate

Calculate principal strains and directions

Calculate compressive (or tensile) damage

Convert to global coordinate

**Fig. 4** Damage calculation process

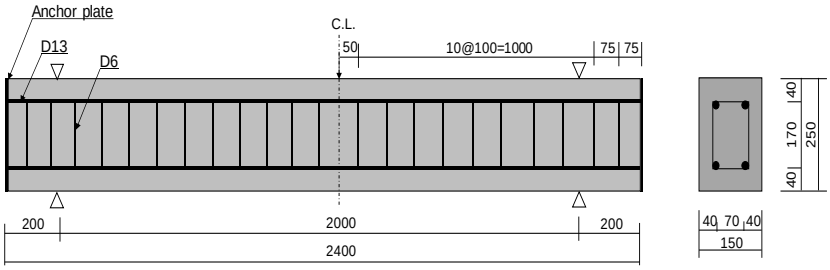


**Fig.7** RC beam model

$$DIF = \frac{f'_{cd}}{f'_{cs}} = \left(\frac{\dot{\varepsilon}}{\dot{\varepsilon}_s}\right)^{0.006\left[\log\left(\frac{\dot{\varepsilon}}{\dot{\varepsilon}_s}\right)\right]^{1.05}}, \quad (10)$$
$$\dot{\varepsilon}_s = 1.2 \times 10^{-5}(s^{-1})$$

$$DIF = \frac{f'_{td}}{f'_{ts}} = \exp\left[0.00126\left(\log\frac{\dot{\varepsilon}}{\dot{\varepsilon}_s}\right)^{3.373}\right], \quad (11)$$
$$\dot{\varepsilon}_s = 1.0 \times 10^{-7}(s^{-1})$$

Where $f'_{cd}$ is the dynamic compressive strength, $f'_{cs}$ is the static compressive strength, $f'_{td}$ is the dynamic tensile strength, and $f'_{ts}$ is the static tensile strength.

For the steel material, von Mises yield criterion is used, and strain hardening exponent is introduced to describe the hardening process. The uniaxial stress-strain relationship of steel is shown in Fig.6. Since the influence of the strain rate effect is relatively small, Takahashi's equation[13] is adopted, shown in Eq. (12).

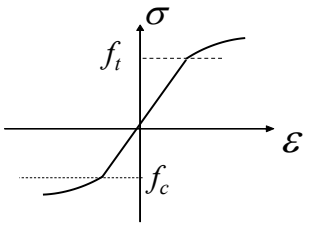


**Fig. 6** Uniaxial stress-strain relationship of steel

$$DIF = \frac{f'_{yd}}{f'_{ys}} = 1.202 + 0.040log(\dot{\varepsilon}), \quad (12)$$
$$(\dot{\varepsilon} \geq 5.0 \times 10^{-5})$$

Where $f'_{yd}$ is the dynamic yielding strength, $f'_{ys}$ is the static yielding strength.

## 3. ANALYSIS FOR RC BEAM IMPACT PROBLEM

### 3.1 Analysis object

Fig.7. shows the geometry of analysis object RC beam and its arrangement. In the experiment, the size of RC beam was 150 × 250 mm (beam width × beam height) with a total length of 2400 mm. Four D13 main rebars were arranged at the position of 40 mm from the upper and lower ends and D6 rebars were arranged every 100 mm as shear reinforcements. In addition, a 300 kg columnar steel weight was used to collide against the upper central surface of the RC beam. Material properties of steel rebars and concrete are shown in Table 1, and the erosion limit is set to 6%.

**Table 1** Material properties

| Material | Rebar | | Concrete |
|---|---|---|---|
| | D6 | D13 | |
| Density (kg/m3) | 7853 | 7853 | 2500 |
| Young' modulus (kN/mm2) | 206 | 206 | 23.1 |
| Compressive / Yield strength (N/mm2) | 368 | 373 | 25 |
| Tensile strength (N/mm2) | - | - | 2.5 |
| Poisson ratio | 0.30 | 0.30 | 0.23 |

Fig.8. shows the perspective view and the arrangement condition of steel bars in the analytical model. Impact response analyses of RC beams are performed using a 1/2 model where the particle size is 10mm. As for the boundary conditions, the particles of the supporting position on the bottom are constrained in the vertical direction and the particles on the symmetric plane are also constrained in the horizontal direction. In this analysis, supporting jigs of RC beam are not modeled.

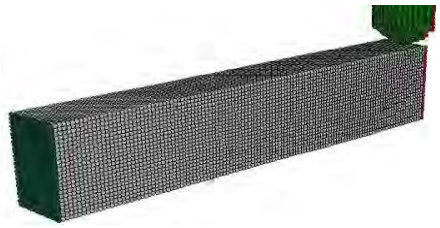

**(a)** Perspective view

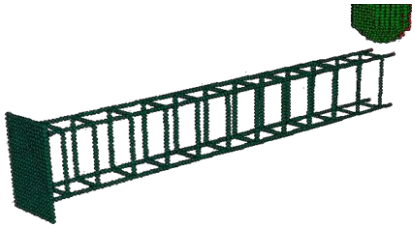

**(b)** steel bars arrangement

**Fig.8** Analysis model of the RC beam

### 3.2 Results and discussion

As for reaction force response, negative reaction force occurs at the first stage as shown in Figure 9(a), this is due to the third bending deformation mode of RC beam and this phenomenon is also reproduced in the analysis. Although the analytical reaction force is reaching the maximum value faster, it is almost equal to the test result. On the other hand, there is a big difference between

the test result and analyses after the maximum reaction force because of the lack of supporting jig in the analysis model. From the displacement response shown in Figure 9(b), it can be found that displacement-time history of the analysis results and experiment results are almost the same, and the difference of residual displacement is a little larger in the case of 4m/s. Figure 10 shows the comparison of crack distribution between experiment and analysis. The maximum principal strain is taken as the value to describe cracks in analysis and its distribution is shown in Figure 10(b). It can be found that although the crack distribution at ends of the beam is not reproduced accurately (due to the difference of reaction forces after their maximum value), the crack distribution in the central span agreed well. From these verifications, it can be said that the impact response analysis by SPH method could predict reliable elastic-plastic impact behavior of RC beam.

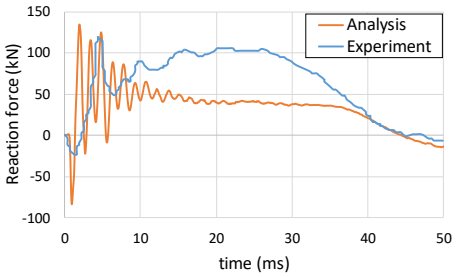


(a) Reaction force response

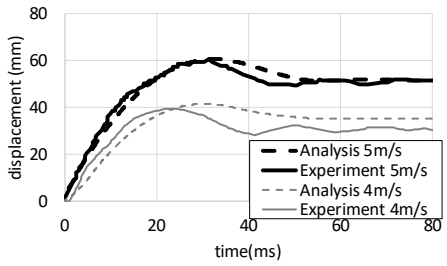


(b) Displacement response

**Fig.9** Comparison of impact responses between analysis and experiment

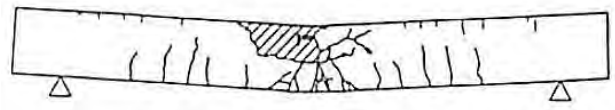

(a) Experiment

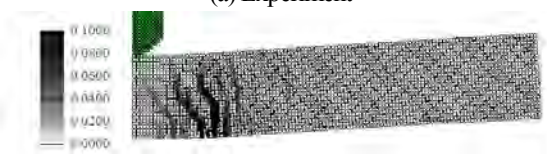

(b) Analysis

**Fig.10** Comparison of crack distribution between analysis and experiment

## 4. RC SLAB PENETRATION ANALYSIS

### 4.1 RC slab analysis model

Figure 11 shows the geometry of the concrete slab used for the analysis. The size of the model is 2000mm×2000mm×200mm. It is assumed that the slab is fixed with four-side simple support by the jigs with 1750 mm spacing. The collision object is 300 kg in weight, whose nose shape is a hemisphere (radius of curvature of 80 mm), and the collision position is the upper center surface of the slab. The impact analysis is performed The material properties of concrete are set as shown in Table 2. For the mechanical characteristic of concrete particles, as shown in Figure 5, the stress-strain relations are set with hardening on the compression side and softening on the tensile side. Impact response analyses of RC slabs are performed using a 1/4 model with the particle size of 10mm, as shown in Figure 11(c). The impact velocity of the projectile varies from 10m/s to 200m/s. The failure mode, impact force, and impulse are investigated from each result and the evaluation method to prevent the penetration of a concrete slab is examined.

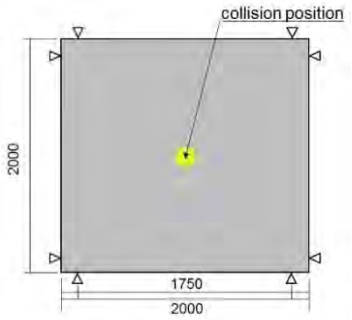


(a) Top view

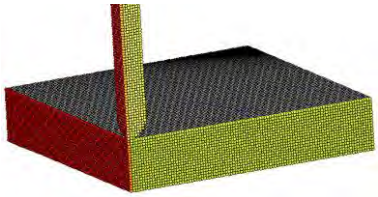

(c) 1/4 model

**Fig.11** Concrete slab in analysis

Table 2. Material property of concrete

| | |
|---|---|
| Mass density (kg/m$^3$) | 2500 |
| Young's modules (kN/mm$^2$) | 29.0 |
| Compressive strength (N/mm$^2$) | 34.1 |
| Tensile strength (N/mm$^2$) | 3.41 |
| Poisson ratio | 0.22 |

### 4.2 Results and discussion

From the impact load response shown in Figure 12, it can be found that the maximum load increases with impact velocity, and load duration decreases with impact velocity. When the impact velocity is higher, the shape of the load response curve is steeper, and the maximum load occurs at an early stage. Next, Figure 13 shows the relationship between the impulse (calculated by the area of impact load-time history) and the impact velocity. From this figure, it is found that there is an obvious tendency between the impact velocity and the impulse. At first, the impulse increases

linearly with the impact velocity (the flying object does not penetrate due to the insufficient impact velocity of 10 m/s ~ 50 m/s). On the other hand, when the flying object collides at a medium velocity (50m/s ~ 150 m/s) and it penetrates the concrete slab, the impulse required for penetration decreases as the initial velocity increases. Furthermore, it is also confirmed that the impulse required for penetration of the concrete slab converge certain value under high-velocity impact condition (more than 150 m/s). These trends are also confirmed under the different mass of the projectile (100kg ~ 300kg).

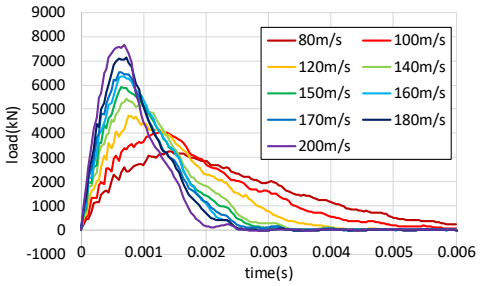


**Fig.12** Influence of projectile velocity to the response of impact force.

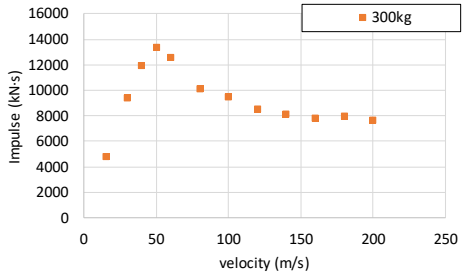


(a) Projectile of 300kg

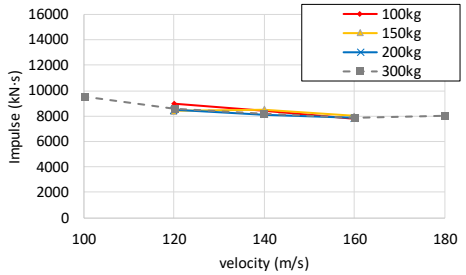


(b) Projectile of different mass

**Fig.13** Comparison of impulses required for penetration

## 5. CONCLUSION

In this study, an analytical method to express the penetration failure of a concrete slab subjected to the collision of a flying object is presented. In addition, the penetration limit of the concrete slab is evaluated by the proposed method. The results of this study are summarized as follows.

1)The impact response and crack distribution of RC beam can be predicted by proposed SPH analysis.

2)The penetration process and load response of concrete slab against high-velocity projectile can be reproduced.

3)It is recognized that impulse (integration of impact load-time history) is an appropriate threshold value for the penetration limit of the concrete slab.

## References


1) U.S. NUCLEAR REGULATORY COMMISSION: REGULATORY GUIDE 1.76, DESIGN-BASIS TORNADO AND TORNADO MISSILES FOR NUCLEAR POWER PLANTS, Revision 1, March 2007
2) Beppu, M., Miwa, K., Itoh, M., Katayama, M. and Ohno, T. : Damage evaluation of concrete plates by high-velocity impact. International Journal of Impact Engineering, 35(12), pp.1419-1426, 2008
3) Kojima, I. : An experimental study on local behavior of reinforced concrete slabs to missile impact. Nuclear Engineering and Design, 130(2): 121-132, 1991
4) Zhang, M. H., Shim, V. P. W., Lu, G., & Chew, C. W. : Resistance of high-strength concrete to projectile impact. International Journal of Impact Engineering, 31(7), 825-841, 2005
5) Kennedy, R. P. : A review of procedures for the analysis and design of concrete structures to resist missile impact effects. Nuclear Engineering and Design, 37(2): 183-203, 1976
6) Libersky, L. D., and Petschek, A. G. : Smooth particle hydrodynamics with strength of materials. In Advances in the free-Lagrange method including contributions on adaptive gridding and the smooth particle hydrodynamics method, pp. 248-257, Springer, Berlin, Heidelberg, 1991
7) Libersky, L. D., Petschek, A. G., Carney, T. C., Hipp, J. R. and Allahdadi, F. A. : High strain Lagrangian hydrodynamics: a three-dimensional SPH code for dynamic material response. Journal of computational physics, 109(1): 67-75, 1993
8) Monaghan, J. J. : Simulating free surface flows with SPH. Journal of computaional physics, 110(2), 399-406, 1994
9) Japan Society of Civil Engineers Concrete Committee, 2012. Standard specifications for concrete structures: Design, pp.37-38. (In Japanese)
10)Popovics, S. : A numerical approach to the complete stress-strain curve of concrete. Cement and concrete research, 3(5): 583-599, 1973
11)Fujikake, K., Shinozaki, Y., Ohno, T., Mizuno, J. and Suzuki, A. : Post-peak and strain-softening behaviors of concrete materials in compression under rapid loading. Journal of JSCE, 1999(627): 37-54. (In Japanese)
12)Ross, C. A. and Tedesco, J. W. : Split-Hopkinson pressure-bar tests on concrete and mortar in tension and compression. Materials Journal, 86(5): 475-481. 1989
13)Takahashi, Y., Ohno, T., Ohta, T. and Hino, S. : Method for Estimating Ultimate Limit Deformation of Reinforced Concrete Beams Under High Speed Loadings. Journal of JSCE, 1991(432): 99-108. (In Japanese)